Dynamic Electrophoretic Mobility of Concentrated Dispersions of Spherical Colloidal Particles. On the Consistent Use of the Cell Model

S. Ahualli,[†] A. Delgado,[†] S. J. Miklavcic,*[,‡] and L. R. White[§]

Departamento de Fisica Aplicada, Facultad de Ciencias, Universidad de Granada, Granada, Spain, Department of Science and Technology, University of Linköping, S-601 74, Norrköping, Sweden, and Department of Chemical Engineering, Carnegie Mellon University, Pittsburgh, Pennsylvania

Received March 17, 2006. In Final Form: May 30, 2006

This paper outlines a complete and self-consistent cell model theory of the electrokinetics of dense spherical colloidal suspensions for general electrolyte composition, frequency of applied field, ζ potential, and particle size. The standard electrokinetic equations, first introduced for any given particle configuration, are made tractable to computation by averaging over particle configurations. The focus of this paper is on the systematic development of suitable boundary conditions at the outer cell boundary obtained from global constraints on the suspension. The approach is discussed in relation to previously published boundary conditions that have often been introduced in an ad hoc manner. Results of a robust numerical calculation of high-frequency colloidal transport properties, such as dynamic mobility, using the present model are presented and compared with some existing dense suspension models.

I. Introduction

The advent of electroacoustic methods for measuring electrophoretic mobility and dielectric spectroscopy in the megahertz frequency regime has enabled the experimentalist to probe the surface charge and size distribution of suspension particles at volume fractions inaccessible to optical techniques. This has led to the online monitoring of dense commercial suspensions such as emulsions and chemical mechanical polishing slurries.[1] For process control, it may be sufficient to simply follow the measured quantity of interest, for example, the electrophoretic mobility, μ, or dipole strength, d. However, for a fuller understanding of the surface charging and suspension stability, it is necessary to have a theory that relates the measured quantity to the surface charge properties of the particle. Electrokinetic theory for dilute suspensions is well developed,[1−12] but this is not yet the case for dense suspensions.

For thin double-layer systems ($\kappa a \gg 1$, where a is the particle radius and κ^{-1} is the Debye screening length in the bathing electrolyte), there has been some progress using the properties of a neutrally buoyant suspension[13] and more systematic methods[14,15] involving exact calculations of the electrokinetic properties to next order in volume fraction, ϕ, or a spherical harmonic expansion treatment of the fields around each particle[16] in random arrays. The electrokinetic properties for regular arrays of particles have also been calculated.[3,4,16] For large κa suspensions, for which the double layer can be treated as a surface layer of negligible thickness, the particles are not strongly interacting in the unperturbed state, and it is sufficient to consider only the linear superposition of the perturbation fields. On the other hand, there is growing interest in small κa systems due to the processing requirements of nanoparticulate suspensions in water (small a) and the electrophoretic behavior of nonaqueous suspensions such as soot-laden engine oils or electronic inks (small κ). For such systems, the methods discussed above are difficult to implement because the equilibrium double layers can overlap significantly.

The present paper addresses the task of developing a general theory of electrokinetics in dense suspensions valid for arbitrary electrolyte composition, ζ potential, ζ, and general κa. Specifically, we examine the cell model as a candidate for this general theory. Figure 1 illustrates the essential features of the cell model approximation: a dense suspension of spherical particles subject to an applied electric field whose volume average is denoted $\langle \mathbf{E} \rangle$. The instantaneous Wigner−Seitz cell surrounding each particle of the suspension upon ensemble averaging is replaced by a spherical bounding surface of radius

$$b = a\phi^{-1/3}$$

such that the average volume fraction is preserved. The cell model approximation has the desirable characteristic that the symmetry of the system is identical to that of an isolated particle in the field $\langle \mathbf{E} \rangle$, so that representations of the perturbation fields developed for the isolated case have immediate application to the cell model. The disadvantage of the model is the necessity of devising suitable outer boundary conditions on the perturbation fields. There are, of course, no boundary conditions pertaining to the instantaneous Wigner−Seitz boundary apart from the continuity constraints on the solutions of the partial differential equations (given below) for the perturbation fields. Thus, the ensemble averaged system does not naturally possess outer boundary conditions at $r = b$, where r is the radial coordinate from the center of the particle, by virtue of the ensemble averaging of any such conditions applicable to the instantaneous Wigner−Seitz boundary.

A number of candidate boundary conditions have been proposed,[17−37] but these have often appeared in an ad hoc fashion,

* Corresponding author.
[†] Universidad de Granada.
[‡] University of Linköping.
[§] Carnegie Mellon University.

(1) Hunter, R. J. *Colloids Surf., A* **1989**, *141*, 37.
(2) O'Brien, R. W.; White, L. R. *J. Chem. Soc., Faraday Trans. 2* **1978**, *74*, 1607.
(3) O'Brien, R. W.; Perrins, W. T. *J. Colloid Interface Sci.* **1984**, *99*, 20.
(4) O'Brien, R. W. *J. Colloid Interface Sci.* **1986**, *113*, 81.
(5) O'Brien, R. W. *J. Colloid Interface Sci.* **1986**, *110*, 477.
(6) O'Brien, R. W. *J. Fluid Mech.* **1988**, *190*, 71.
(7) O'Brien, R. W. *J. Fluid Mech.* **1990**, *212*, 81.
(8) Manglesdorf, C. S.; White, L. R. *J. Chem. Soc., Faraday Trans.* **1992**, *88*, 3567.
(9) Manglesdorf, C. S.; White, L. R. *J. Colloid Interface Sci.* **1993**, *160*, 275.
(10) Rosen, L. A.; Baygents, J. C.; Saville, D. A. *J. Chem. Phys.* **1993**, *98*, 4183.
(11) Ennis-King, J.; White, L. R. *J. Colloid Interface Sci.* **1996**, *178*, 446.
(12) Hunter, R. J. *Foundations of Colloid Science*, 2nd ed.; Oxford University Press: New York, 2001.
(13) O'Brien, R. W.; Jones, A.; Rowlands, W. N. *Colloids Surf.*, A **2003**, *218*, 89.
(14) Ennis-King, J.; White, L. R. *J. Colloid Interface Sci.* **1997**, *185*, 157.
(15) Shugai, A. A.; Carnie, S. L.; Chan, D. Y. C.; Anderson, J. L. *J. Colloid Interface Sci.* **1997**, *191*, 357.
(16) Kang, S.-Y.; Sangani, A. S. *J. Colloid Interface Sci.* **1994**, *165*, 195.
(17) Levine, S.; Neale, G. H. *J. Colloid Interface Sci.* **1974**, *47*, 520.

10.1021/la0607252 CCC: $33.50
Published on Web 07/04/2006

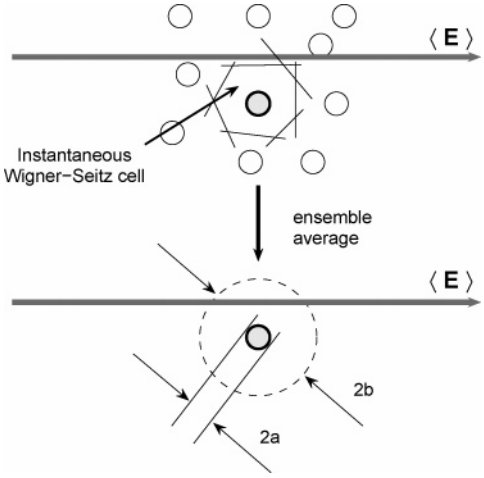

Figure 1. Schematic of a Wigner−Seitz cell surrounding a given spherical particle in a given configuration of particles in a concentrated dispersion, and the imagined spherical cell achieved by ensemble averaging particle positions. The spherical cell has a radius of $b = a\phi^{-1/3}$, where a is the particle radius, and ϕ is the volume fraction of particles. The applied field direction is shown.

and, while they may seem reasonable, they have not always been rigorously motivated. The philosophy we advocate in this paper is that there is one possible source from which to determine the appropriate boundary conditions, and that is the set of global physical constraints that apply unequivocally to the instantaneous system, which must carry over to the ensemble averaged cell model. These global constraints and the corresponding deduced outer boundary conditions are discussed below in relation to previously proposed conditions.

This paper is organized as follows: In the next section we introduce the set of governing equations that would apply for an arbitrary distribution of colloidal particles. We then apply standard linear perturbation theory and separate the equations into two orders: a zeroth-order, field-independent contribution and a first-order, linear field-dependent contribution. The resulting orders of equations are then averaged over all particle positions. Some inherent approximations associated with this averaging process are briefly discussed. Section 4 details the principal contribution of this paper, namely, the global constraints and boundary conditions derived from them. In section 5, we present numerical results produced by the cell model using the correct boundary conditions, and compare these with some other existing cell models. In our derivations, we make reference to a cell average (of a generic function, f) of the form

$$\langle f(\mathbf{r})\rangle = \frac{1}{V}\int_V f(\mathbf{r})\mathrm{d}V$$

where V is the cell volume made up of both the particle volume, V_p, and the fluid volume, V_s.

II. The Standard Model of Colloidal Electrokinetics

When an electric field $\langle \mathbf{E}(t)\rangle$ is applied to a colloidal suspension, the electrolyte ion number densities, n_j, electrochemical potentials, μ_j, drift velocities, $\mathbf{v}_j$ ($j = 1, 2, ..., N$), the hydrodynamic flow field, $\mathbf{u}$, pressure, p, and electrostatic potential, Ψ, are described by the following fundamental equations:[4,6,7]

$$\nabla^2\Psi(\mathbf{r},t) = -\frac{1}{\epsilon_s\epsilon_0}\rho(\mathbf{r},t) \quad (1)$$

$$\rho_s\frac{\partial \mathbf{u}}{\partial t}(\mathbf{r},t) = -\nabla p(\mathbf{r},t) - \rho(\mathbf{r},t)\nabla\Psi(\mathbf{r},t) + \eta_s\nabla^2\mathbf{u}(\mathbf{r},t) \quad (2)$$

$$\nabla\cdot\mathbf{u}(\mathbf{r},t) = 0 \quad (3)$$

$$\mathbf{v}_j(\mathbf{r},t) = \mathbf{u}(\mathbf{r},t) - \frac{1}{\lambda_j}\nabla\mu_j(\mathbf{r},t) \quad (4)$$

$$\frac{\partial n_j}{\partial t}(\mathbf{r},t) + \nabla\cdot[n_j(\mathbf{r},t)\mathbf{v}_j(\mathbf{r},t)] = 0 \quad (5)$$

$$\mu_j(\mathbf{r},t) = -z_j e\Phi_j(\mathbf{r},t) = \mu_j^{\infty} + z_j e\Psi(\mathbf{r},t) + k_B T\ln[n_j(\mathbf{r},t)] \quad (6)$$

with charge density

$$\rho(\mathbf{r},t) = \sum_{j=1}^{N} z_j e n_j(\mathbf{r},t) \quad (7)$$

Here, e, ϵ_s, ϵ_0, ρ_s, η_s, z_j, λ_j, k_B, and T are the electron charge, the relative fluid dielectric permittivity, vacuum permittivity, fluid mass density, fluid viscosity, valency and ionic drag coefficients of the jth ion type, Boltzmann constant, and temperature, respectively. The drag coefficient, λ_j, is related to the ionic limiting conductance, Λ_j^{∞}, by

$$\lambda_j = \frac{N_A e^2|z_j|}{\Lambda_j^{\infty}} \quad (8)$$

where N_A is Avogadro's number.

In the Navier−Stokes equations for the fluid flow field (eqs 2 and 3), the velocity, $\mathbf{u}$, is assumed to be sufficiently small that the quadratic inertial terms in the momentum balance can be neglected. As will be shown below, the electrochemical potential functions, $\Phi_j(\mathbf{r},t)$, introduced in eq 6, represent the deviations of the local ion densities from their (equilibrium) Poisson−Boltzmann expressions in terms of the local electrostatic potential, $\Psi(\mathbf{r},t)$. Equations 5 and 6 may be combined to give

$$\nabla^2\Phi_j - \frac{\lambda_j}{k_B T}\frac{\partial}{\partial t}(\Phi_j + \Psi) = \frac{e}{k_B T}(\nabla\Phi_j + \nabla\Psi)\cdot\left(z_j\nabla\Phi_j + \frac{\lambda_j}{e}\mathbf{u}\right) \quad (9)$$

(18) Kozak, M. W.; Davis, E. J. *J. Colloid Interface Sci.* **1986**, *112*, 403.
(19) Kozak, M. W.; Davis, E. J. *J. Colloid Interface Sci.* **1989**, *127*, 497.
(20) Kozak, M. W.; Davis, E. J. *J. Colloid Interface Sci.* **1989**, *129*, 166.
(21) Shilov, V. N.; Zharkikh, N. I.; Borkovskaya, Y. B. *Kolloidn. Zh.* **1981**, *43*, 434.
(22) Zharkikh, N. I.; Shilov, V. N. *Kolloidn. Zh.* **1981**, *43*, 1061.
(23) Shilov, V. N.; Borkovskaya, Y. B. *Kolloidn. Zh.* **1994**, *56*, 647.
(24) Dukhin, A. S.; Shilov, V. N.; Borkovskaya, Y. B. *Langmuir* **1999**, *15*, 3452.
(25) Dukhin, A. S.; Shilov, V. N.; Ohshima, H.; Goetz, P. J. *Langmuir* **1999**, *15*, 6692.
(26) Dukhin, A. S.; Ohshima, H.; Shilov, V. N.; Goetz, P. J. *Langmuir* **1999**, *15*, 3445.
(27) Ohshima, H. *J. Colloid Interface Sci.* **1997**, *188*, 481.
(28) Ohshima, H. *J. Colloid Interface Sci.* **1997**, *195*, 137.
(29) Lee, E.; Chu, J. W.; Hsu, J. *J. Colloid Interface Sci.* **1999**, *209*, 481.
(30) Lee, E.; Chu, J. W.; Hsu, J. *J. Chem. Phys.* **1999**, *110*, 11643.
(31) Ding, J. M.; Keh, H. J. *J. Colloid Interface Sci.* **2001**, *236*, 180.
(32) Carrique, F.; Arroyo, F. J.; Delgado, A. V. *Colloids Surf., A* **2001**, *195*, 157
(33) Carrique, F.; Arroyo, F. J.; Delgado, A. V. *J. Colloid Interface Sci.* **2001**, *243*, 351.
(34) Carrique, F.; Arroyo, F. J.; Delgado, A. V. *J. Colloid Interface Sci.* **2002**, *252*, 126.
(35) Carrique, F.; Arroyo, F. J.; Jimenez, M. L.; Delgado, A. V. *J. Chem. Phys.* **2003**, *118*, 1945.
(36) Arroyo, F. J.; Carrique, F.; Ahualli, S.; Delgado, A. V. *Phys. Chem. Chem. Phys.* **2004**, *6*, 1446.
(37) Hill, R. J.; Saville, D. A.; Russel, R. B. *J. Colloid Interface Sci.* **2003**, *258*, 56.

These are the basic equations, which hold everywhere in the fluid between the colloidal particles. To make this system tractable, we seek a perturbation expansion in the form

$$\Xi(\mathbf{r},t) = \Xi^{(0)}(\mathbf{r}) + \Xi^{(1)}(\mathbf{r},t) + O(\langle \mathbf{E}(t)\rangle^2) \tag{10}$$

where Ξ represents any of the field variables, Φ_j, Ψ, $\mathbf{u}$, ρ, n_j, and p, with $\Xi^{(0)}$ representing the respective field-independent equilibrium contributions and $\Xi^{(1)}$ representing the contributions that are linearly dependent on the average external field, $\langle \mathbf{E}(t)\rangle$. For an oscillatory applied field,

$$\langle \mathbf{E}(t)\rangle = \langle \mathbf{E}\rangle e^{-i\omega t} \tag{11}$$

the first-order contributions to the perturbed fields can be expressed as a linear response,

$$\Xi^{(1)}(\mathbf{r},t) = \Xi^{(1)}(\mathbf{r})e^{-i\omega t} \tag{12}$$

where $\Xi^{(1)}(\mathbf{r})$ is linearly proportional to $\langle \mathbf{E}\rangle$ (see later). By inserting expansion 10 into the field equations, eqs 1−9, we obtain a hierarchy of equations that must be solved to obtain the electrokinetic properties of interest.

III. Governing Equations

A. The Zeroth-Order Problem. An ensemble averaging over all particle configurations, denoted by $\overline{(\cdot)}$, leads to a cell model system of spherical particles. In obtaining equations for equilibrium quantities, we introduce the additional approximation that $\overline{f(\Xi(\mathbf{r}))} = f(\overline{\Xi(\mathbf{r})})$ for an arbitrary functional, f, and arbitrary field variable, Ξ, which is reasonable for the case of thin, nonoverlapping double layers, when $\kappa a \gg 1$, but diminishes in accuracy as κa gets smaller. However, to avoid the approximation altogether, one must resort to a complicated statistical mechanical description, which would then be inconsistent with the mean-field treatment of the statistical mechanics of electrolyte ions. The cell model approximation at least has the virtue of computational simplicity. In the absence of an applied electric field, computations are confined to a mathematical cell enclosing an arbitrary charged particle and are functions only of the spherical radial coordinate, r. To zeroth-order in the applied electric field, the field equations are then

$$\begin{cases} n_j^{(0)}(r) = n_j^{\infty}\exp(-z_j e\Psi^{(0)}(r)/k_B T), \\ \rho^{(0)}(r) = \sum_{j=1}^{N} z_j e n_j^{(0)}(r), \end{cases} \tag{13}$$

$$p^{(0)}(r) = p_{amb} + \sum_{j=1}^{N}(n_j^{(0)}(r) - n_j^{\infty})k_B T \tag{14}$$

$$\mu_j^{(0)}(r) = -z_j e\Phi_j^{(0)}(r) = \mu_j^{\infty} + k_B T \ln n_j^{\infty} \tag{15}$$

$$\frac{1}{r^2}\frac{d}{dr}\left(r^2\frac{d\Psi^{(0)}}{dr}(r)\right) = \begin{cases} 0 & r < a \\ -\dfrac{\rho^{(0)}(r)}{\epsilon_s\epsilon_0}, & a < r < b \end{cases} \tag{16}$$

In eq 14, p_{amb} is the ambient pressure outside the double layer. The ion densities, n_j^{∞}, are those of a reservoir electrolyte that is in equilibrium with the suspension. Experimentally, the n_j^{∞} are determined by dialyzing the suspension against a known electrolyte reservoir.

At each particle surface (i.e., the "slipping plane"), $r = a$, the rest electric potential satisfies

$$\Psi^{(0)}|_{r=a} = \zeta \tag{17}$$

where it has been assumed that the zeta potential, ζ, does not vary around the particle surface. Inside the particle, eqs 16 and 17 yield

$$\Psi^{(0)}(r) = \zeta \tag{18}$$

so that the equilibrium surface charge density, $\sigma^{(0)}$, is given by

$$\sigma^{(0)} = -\epsilon_0\epsilon_s\left.\frac{d\Psi^{(0)}}{dr}\right|_{r=a^+} \tag{19}$$

These zeroth-order equations apply in the electrolyte between the instantaneous particle positions.

The global electroneutrality constraint is

$$\langle \rho^{(0)}(\mathbf{r})\rangle = \frac{1}{V}\int_V \rho^{(0)}(\mathbf{r})dV$$

$$= -\frac{\epsilon_s\epsilon_0}{V}\int_V \nabla^2\Psi^{(0)}(\mathbf{r})dV = 0$$

which, from Green's theorem applied to the cell volume, produces the outer boundary condition

$$\left.\frac{d\Psi^{(0)}}{dr}\right|_{r=b} = 0 \tag{20}$$

This boundary condition is an example of an outer boundary condition derived from a global constraint. We continue with this same working principle for the first-order problem discussed in the next subsection.

Equations 16, 17, and 20 serve to determine the equilibrium cell model.

B. The First-Order Problem. The first-order field equations are

$$\nabla^2\Psi^{(1)}(\mathbf{r}) = -\frac{1}{\epsilon_s\epsilon_0}\rho^{(1)}(\mathbf{r}) \tag{21}$$

where

$$\rho^{(1)}(\mathbf{r}) = \sum_{j=1}^{N} z_j e n_j^{(1)}(\mathbf{r}) \tag{22}$$

and

$$n_j^{(1)}(\mathbf{r}) = -\frac{z_j e}{k_B T}n_j^0(r)[\Phi_j^{(1)}(\mathbf{r}) + \Psi^{(1)}(\mathbf{r})] \tag{23}$$

$$\nabla^2\Phi_j^{(1)}(\mathbf{r}) + \frac{i\omega\lambda_j}{k_B T}(\Phi_j^{(1)}(\mathbf{r}) + \Psi^{(1)}(\mathbf{r})) = \frac{e}{k_B T}\frac{d\Psi^{(0)}}{dr}(r)\left(z_j\frac{\partial\Phi_j^{(1)}(\mathbf{r})}{\partial r} + \frac{\lambda_j}{e}\mathbf{u}^{(1)}(\mathbf{r})\cdot\hat{\mathbf{r}}\right) \tag{24}$$

$$\nabla\cdot\mathbf{u}^{(1)}(\mathbf{r}) = 0 \tag{25}$$

and

$$\eta_s\nabla^2\mathbf{u}^{(1)}(\mathbf{r}) - \nabla p^{(1)}(\mathbf{r}) + i\omega\rho_s\mathbf{u}^{(1)}(\mathbf{r}) = \rho^{(0)}(r)\nabla\Psi^{(1)}(\mathbf{r}) + \rho^{(1)}(\mathbf{r})\frac{d\Psi^{(0)}}{dr}(r)\hat{\mathbf{r}} \tag{26}$$

These linear equations hold in the electrolyte between the

instantaneous particle positions. To make this system tractable to computation, we ensemble average over all particle configurations. At this level, the cell model makes the additional approximation that

$$\overline{(\Xi_1(\mathbf{r})\Xi_2(\mathbf{r}))} = \overline{(\Xi_1(\mathbf{r}))\cdot(\Xi_2(\mathbf{r}))}$$

Fortunately, the quadratic terms that appear in eqs 21−26 (and require this approximation) vanish outside the double layer about each particle so that, when $\kappa a \gg 1$, the zeroth-order fields become independent of particle configurations, and this approximation is valid.

The dipolar symmetry of the electrokinetic cell model problem suggests the definition

$$\Xi^{(1)}(\mathbf{r}) = \xi(r)\langle\mathbf{E}\rangle\cdot\hat{\mathbf{r}} \tag{27}$$

where $\Xi^{(1)}(\mathbf{r})$ represents the first-order quantities $\Psi^{(1)}(\mathbf{r}), \Phi_j^{(1)}(\mathbf{r})$, and $p^{(1)}(\mathbf{r})$; and $\xi(r)$ represents the corresponding coefficient functions $\psi(r)$, $\phi_j(r)$, and $P(r)$. Furthermore, following[38] the symmetry requires that the fluid velocity (in the reference frame of the central particle) takes the form

$$\mathbf{u}^{(1)}(\mathbf{r}) = (u_r, u_\theta, u_\phi) = \mu(\omega)\langle\mathbf{E}\rangle - \left(\frac{2h(r)}{r}\langle\mathbf{E}\rangle\cdot\hat{\mathbf{r}}, \frac{1}{r}\frac{\partial(rh(r))}{\partial r}[\langle\mathbf{E}\rangle - \langle\mathbf{E}\rangle\cdot\hat{\mathbf{r}}\hat{\mathbf{r}}], 0\right) \tag{28}$$

The first-order cell model is the solution of the coupled set of complex ordinary differential equations for the functions ψ, ϕ_j, and the newly introduced h:[4]

$$L\psi(r) = \frac{e^2}{\epsilon_s\epsilon_0 k_B T}\sum_{j=1}^{N} z_j^2 n_j^0(r)[\phi_j(r) + \psi(r)] \tag{29}$$

$$L\phi_j(r) + \gamma_j^2[\phi_j(r) + \psi(r)] = \frac{e}{k_B T}\frac{d\Psi^{(0)}}{dr}(r)\left(z_j\frac{d\phi_j(r)}{dr} - \frac{2\lambda_j}{e}\frac{h(r)}{r}\right) \tag{30}$$

and

$$L(L + \gamma^2)h(r) = -\frac{e^2}{\eta_s k_B T}\frac{1}{r}\frac{d\Psi^{(0)}}{dr}\sum_{j=1}^{N} z_j^2 n_j^0(r)\phi_j(r) \tag{31}$$

where we have introduced the constants

$$\gamma = (1+i)\sqrt{\frac{\omega\rho_s}{\eta_s}}, \gamma_j = (1+i)\sqrt{\frac{\omega\lambda_j}{k_B T}} \tag{32}$$

and the second-order differential operator

$$L = \frac{d^2}{dr^2} + \frac{2}{r}\frac{d}{dr} - \frac{2}{r^2} \tag{33}$$

The first-order pressure is[28]

$$p^{(1)}(\mathbf{r}) = P(r)\langle\mathbf{E}\rangle\cdot\hat{\mathbf{r}} \tag{34}$$

where

$$P(r) = -\eta_s\left[\frac{d}{dr}[r(L+\gamma^2)h(r)] - \mu\gamma^2 r + \frac{\rho^{(0)}(r)\psi(r)}{\eta_s}\right] \tag{35}$$

and the fluid stresses (made use of in the next section) are

$$\begin{cases}\sigma_{rr} = -\left[P(r) - 2\eta_s\left(\frac{2}{r}\frac{dh(r)}{dr} - \frac{2}{r^2}h(r)\right)\right]\langle\mathbf{E}\rangle\cdot\hat{\mathbf{r}} \\ \sigma_{r\theta} = \eta_s\frac{d^2h(r)}{dr^2}(\langle\mathbf{E}\rangle - \langle\mathbf{E}\rangle\cdot\hat{\mathbf{r}}\hat{\mathbf{r}}\end{cases} \tag{36}$$

IV. Boundary Conditions for the First-Order Problem

A. Cell Model Inner Boundary Conditions. Four unequivocal boundary conditions can be obtained by applying three physical conditions at the particle surface. At the surface of the particle, that is, at slipping plane, $r = a$, the hydrodynamic "stick" boundary condition requires that the fluid velocity vanish, $\mathbf{u} = 0$, in a frame of reference fixed on the particle center. Since both velocity components—$u_r(a)$ and $u_\theta(a)$—vanish, eq 28 yields the conditions

$$h(a) = \frac{dh}{dr}|_{r=a} = 0 \tag{37}$$

Furthermore, at the surface of the solid particle, the physical condition of no ion penetration must hold. From eqs 5 and 6, the formal statement of zero normal ion flux, $\mathbf{v}_j\cdot\hat{\mathbf{n}} = 0$ at $r = a$, where $\hat{\mathbf{n}}$ is the outward pointing unit surface normal, becomes

$$\frac{d\phi_j}{dr}|_{r=a} = 0 \tag{38}$$

Finally, the continuity of potential and normal electric displacement at the particle surface

$$\begin{cases}\Psi^{(1)}(a^-) = \Psi^{(1)}(a^+), \\ \epsilon_p(\nabla\Psi^{(1)}\cdot\hat{\mathbf{n}})|_{a^-} = \epsilon_s(\nabla\Psi^{(1)}\cdot\hat{\mathbf{n}})|_{a^+}\end{cases}$$

together imply

$$\frac{d\psi}{dr}|_{r=a} - \frac{\epsilon_p}{\epsilon_s a}\psi(a) = 0 \tag{39}$$

We assume here that no change occurs in the charge density behind the slipping plane. This is consistent with the zero ion flux condition. The hydrodynamic, no-slip condition can be relaxed to allow Stern-layer conductance if required.[39]

B. Cell Model Outer Boundary Conditions. It is clear from the orders of the governing differential equations and the number of available conditions that we still require one boundary condition on $\psi(r)$, one for each of the $\phi_j(r)$ values and two for $h(r)$ to uniquely specify the solution of the system. Moreover, it is logical that these should apply at the outer cell boundary, $r = b$. However, arriving at the "correct" outer boundary conditions is not an unambiguous task. In fact, there are nearly as many choices of outer boundary conditions in the electrokinetic cell model literature as there are publications. Since one of the principal contributions of this paper is the implementation of appropriate boundary conditions, we discuss this topic in some detail. We argue that, in the context of the cell model, we are only allowed to invoke global physical constraints, which hopefully will lead to the required outer boundary conditions.

(38) Landau, L. D.; Lifshitz, E. M. *Course of Theoretical Physics: Fluid Mechanics*, 2nd ed.; Pergamon Press: Oxford, 1987; Vol. 6.

(39) Mangelsdorf, C. S.; White, L. R. *J. Chem. Soc., Faraday Trans.* **1998**, *94*, 2441.

The global constraint most universally agreed upon in the literature, and the first one we utilize, is the definition of the governing electric field:

$$\langle -\nabla \Psi^{(1)}(\mathbf{r}) \rangle = \langle \mathbf{E} \rangle \tag{40}$$

Application of Green's theorem to the cell volume average and invoking eq 27 for $\Psi^{(1)}(\mathbf{r})$ yields

$$\psi(b) = -b \tag{41}$$

Most publications use this boundary condition.[17−25,32−37] However, a distinctly different suggestion is Ohshima's condition[27,28] that (in our notation) $-\nabla\, \Psi^{(1)}(r = b) = \langle \mathbf{E} \rangle$, which leads to the Neumann condition $\mathrm{d}\psi/\mathrm{d}r = -1$ at $r = b$. Other choices have also been proposed.[17−20] We take the view that eq 41 is not in doubt. The next global constraint we impose is

$$\langle \nabla n_j^{(1)}(\mathbf{r}) \rangle = 0 \tag{42}$$

This is a stipulation that particle diffusiophoresis is suppressed and that electrophoretic mobility is the only physical result of the oscillating field. Application of Green's theorem to the cell volume average gives

$$n_j^{(1)}(b) = 0 \tag{43}$$

which, from eqs 23 and 41, gives

$$\phi_j(b) = b \tag{44}$$

Boundary condition 43 has been employed in the cell model literature, but with little justification.[29,30] Although other boundary conditions have been proposed,[27,28,31] we take the view that eq 42, or, equivalently, eq 44, is not in dispute.

The two remaining boundary conditions still to be determined involve the flow field, **u**. The hydrodynamic conditions that are to be applied at the outer extreme of the cell are not straightforward to foresee. The difficulty lies in the fact that the true time and space dependence of the flow field requires well-defined positions of the particles, even if the latter are mobile. This true picture is not consistent with the approximation found upon performing an ensemble average of the particle positions prior to solving the hydrodynamic equations. Even so, a number of flow field outer boundary conditions have been proposed in the cell model literature with limited rigorous justification, viz., (i) Happel condition[40]

$$\sigma_{r\theta}|_{r=b} = 0 \tag{45}$$

(ii) Kuwabara condition #1[41]

$$(\nabla \times \mathbf{u})|_{r=b} = 0 \tag{46}$$

(iii) Shilov−Zharkikh condition[22]

$$(\nabla p)|_{r=b} = 0 \tag{47}$$

(iv) Mehta−Morse condition[42]

$$(\mathbf{u} \times \langle \mathbf{E} \rangle)|_{r=b} = 0 \tag{48}$$

All of the above proposals are local conditions that seem physically reasonable in a truly static context but cannot be formulated from global arguments. For example, if one considers a regular array of particles, then straightforward reasoning will show that the Morse−Mehta condition will hold by virtue of symmetry. As said, it is, however, not derivable from a global constraint.

Kuwabara also introduced another intuitive condition at the outer cell boundary:

(v) Kuwabara condition #2[41]

$$u_r|_{r=b} = 0 \tag{49}$$

involving only the radial component of **u**. This condition, it turns out, can be associated with a global constraint based on a different premise. The appropriate global constraint is

$$\langle \mathbf{u}(\mathbf{r}) \rangle = 0 \tag{50}$$

which is the statement that there is no net flow of suspension into or out of a given cell. It is straightforward to demonstrate from representation 28 that

$$\langle \mathbf{u} \rangle = \mu \langle \mathbf{E} \rangle - \frac{2h(b)}{b} \langle \mathbf{E} \rangle \tag{51}$$

so that the appropriate outer boundary condition is that

$$\mu = \frac{2h(b)}{b} \tag{52}$$

This boundary condition has been used without adequate motivation by several authors.[24,25,27,28,32−36] Their use of eq 52 arises from their implementing eq 49. However, we see from eq 28 that the radial component of the flow field in the laboratory frame is itself $[\mu - 2h(b)/b]\langle \mathbf{E} \rangle \cdot \hat{\mathbf{r}}$, so that eq 49 is implied by the application of eqs 50 and 51, and *not* the other way around.

The final global constraint we propose is novel but physically compelling:

$$\langle \nabla p(\mathbf{r}) \rangle = 0 \tag{53}$$

It is the stipulation that no net momentum flux arises within a cell, so that the particle velocity is purely electrophoretic and contains no convective (pressure-driven) contribution. Again, applying Green's theorem to the cell volume average yields

$$P(b) = 0 \tag{54}$$

which, from eq 35, gives our final outer boundary condition,

$$\frac{\mathrm{d}}{\mathrm{d}r}[r(L + \gamma^2)h]|_{r=b} - \mu\gamma^2 b - \frac{\rho^{(0)}(b)b}{\eta_s} = 0 \tag{55}$$

This outer boundary condition has not appeared previously in the cell model literature. Shilov and Zharkikh[22−26] instead proposed the outer pressure gradient condition eq 47 to suppress convection. While this is likely a necessary approximation for the case when $\kappa a \gg 1$, when there is no double-layer overlap, eq 53 is the more generally applicable condition.

Since the a priori unknown electrophoretic mobility explicitly appears in the latter two outer boundary conditions, the set of outer boundary conditions derived from global constraints must be supplemented by an additional equation involving μ. The majority of existing cell model theories correctly use the force balance on the cell as this extra equation, viz.,

$$\int_{S_s:r=b} \sigma \cdot \hat{\mathbf{r}}\, \mathrm{d}\mathbf{S} = -i\omega \left[\frac{4\pi}{3} a^3 \rho_p \mu \langle \mathbf{E} \rangle + \rho_s \int_{V_s} \mathbf{u}(\mathbf{r})\, \mathrm{d}V \right] \tag{56}$$

(40) Happel, J. *AIChE J.* **1958**, *4*, 197.
(41) Kuwabara, S. *J. Phys. Soc. Jpn.* **1959**, *47*, 527.
(42) Mehta, G. D.; Morse, T. F. *J. Chem. Phys.* **1975**, *63*, 1878.

Table 1. A Comparative Summary of the Cell Model Boundary Conditions that Have Appeared in the Literature and Those that Are Proposed in This Work

	$\mathbf{u}(\mathbf{r},t)$	$\Psi^{(1)}(\mathbf{r})$	$\Phi_j^{(1)}(\mathbf{r})$	other conditions
Ohshima[27,28]	$\mathbf{u}\cdot\hat{\mathbf{r}}\|_{r=b} = -\mu\langle E\rangle\cos\theta \Rightarrow \mu = 2h(b)/b$ $(\nabla\times\mathbf{u})\|_{r=b} = 0 \Rightarrow Lh(b) = 0$	$-\nabla\Psi^{(1)}\cdot\hat{\mathbf{r}} = -\langle E\rangle\cos\theta \Rightarrow \mathrm{d}\psi/\mathrm{d}r\|_{r=b} = -1$	For low ζ and $\epsilon_p \ll \epsilon_s$, $n_j^{(1)}(\mathbf{r}) = 0 \Rightarrow \mathrm{d}\phi_j/\mathrm{d}r\|_{r=b} = 1$	$\int_{S_s:r=b}\sigma\cdot\hat{\mathbf{r}}\mathrm{d}\mathbf{S} = -i\omega\left[\frac{4\pi}{3}a^3\rho_p\mu\langle\mathbf{E}\rangle + \rho_s\int_{V_s}\mathbf{u}(\mathbf{r})\mathrm{d}V\right] \Rightarrow$ $\frac{\gamma^2h(b)}{b}\left[1-\frac{2\phi(\rho_p-\rho_s)}{\rho_s}\right] - \left.\frac{\mathrm{d}(Lh+\gamma^2h)}{\mathrm{d}r}\right\|_{r=b} + \frac{\rho^{(0)}(b)}{\eta_s} = 0$
Carrique, Arroyo, Jimenez, Delgado[32−36]	$\mathbf{u}\cdot\hat{\mathbf{r}}\|_{r=b} = -\mu\langle E\rangle\cos\theta \Rightarrow \mu = 2h(b)/b$ $(\nabla\times\mathbf{u})\|_{r=b} = 0 \Rightarrow Lh(b) = 0$	$\Psi^{(1)}(b) = -\langle\mathbf{E}\rangle\cdot\hat{\mathbf{r}} \Rightarrow \psi(b) = -b$	$n_j^{(1)}(b) = 0 \Rightarrow \phi_j(b) = b$	$\int_{S_s:r=b}\sigma\cdot\hat{\mathbf{r}}\mathrm{d}\mathbf{S} = -i\omega\left[\frac{4\pi}{3}a^3\rho_p\mu\langle\mathbf{E}\rangle + \rho_s\int_{V_s}\mathbf{u}(\mathbf{r})\mathrm{d}V\right] \Rightarrow$ $\frac{\gamma^2h(b)}{b}\left[1-\frac{2\phi(\rho_p-\rho_s)}{\rho_s}\right] - \left.\frac{\mathrm{d}(Lh+\gamma^2h)}{\mathrm{d}r}\right\|_{r=b} + \frac{\rho^{(0)}(b)}{\eta_s} = 0$
Shilov−Zharkikh[21,22] Morse−Mehta[42]	$\mathbf{u}\cdot\hat{\mathbf{r}}\|_{r=b} = -\mu\langle E\rangle\cos\theta \Rightarrow \mu = 2h(b)/b$ $(\mathbf{u}\times\langle\mathbf{E}\rangle)\|_{r=b} = 0 \Rightarrow \mathrm{d}h/\mathrm{d}r\|_{r=b} - h(b)/b = 0$	$\Psi^{(1)}(b) = -\langle\mathbf{E}\rangle\cdot\hat{\mathbf{r}} \Rightarrow \psi(b) = -b$	$n_j^{(1)}(b) = 0 \Rightarrow \phi_j(b) = b$	$\int_{S_s:r=b}\sigma\cdot\hat{\mathbf{r}}\mathrm{d}\mathbf{S} = -i\omega\left[\frac{4\pi}{3}a^3\rho_p\mu\langle\mathbf{E}\rangle + \rho_s\int_{V_s}\mathbf{u}(\mathbf{r})\mathrm{d}V\right] \Rightarrow$ $\frac{\gamma^2h(b)}{b}\left[1-\frac{2\phi(\rho_p-\rho_s)}{\rho_s}\right] - \left.\frac{\mathrm{d}(Lh+\gamma^2h)}{\mathrm{d}r}\right\|_{r=b} + \frac{\rho^{(0)}(b)}{\eta_s} = 0$
Dukhin, Shilov, Borkovskaya[24] $\kappa a \gg 1$	$\mathbf{u}\cdot\hat{\mathbf{r}}\|_{r=a} = 0$ $\mathbf{u}\cdot\hat{\theta}\|_{r=b} = -\epsilon_s\epsilon_0/\eta_s\langle\mathbf{E}\rangle\cdot\hat{\theta}$ $(\nabla\times\mathbf{u})\|_{r=b} = 0 \Rightarrow Lh(b) = 0$	$\Psi^{(1)}(b) = -\langle\mathbf{E}\rangle\cdot\hat{\mathbf{r}} \Rightarrow \psi(b) = -b$		$\nabla_{tg}\cdot(\kappa^\sigma\nabla\psi)\|_{r=a} = -K_s\nabla\psi\cdot\hat{\mathbf{r}}\|_{r=a}$ where ∇_{tg} is the surface divergence $\nabla p^{(1)}\|_{r=b} = 0$
this work	$\langle\mathbf{u}(\mathbf{r})\rangle = 0 \Rightarrow \mu = 2h(b)/b$	$\langle-\nabla\Psi^{(1)}(\mathbf{r})\rangle = \langle\mathbf{E}\rangle \Rightarrow \psi(b) = -b$	$\langle\nabla n_j^{(1)}(\mathbf{r})\rangle = 0 \Rightarrow \phi_j(b) = -b$	$\int_{S_s:r=b}\sigma\cdot\hat{\mathbf{r}}\mathrm{d}\mathbf{S} = -i\omega\left[\frac{4\pi}{3}a^3\rho_p\mu\langle\mathbf{E}\rangle + \rho_s\int_{V_s}\mathbf{u}(\mathbf{r})\mathrm{d}V\right] \Rightarrow$ $Lh(b) = \gamma^2b\phi\left(\frac{\rho_p-\rho_s}{\rho_s}\right)h(b)$ $\langle\nabla p^{(1)}(\mathbf{r})\rangle = 0 \Rightarrow P(b) = 0$

where $\sigma e^{-i\omega t}$ is the total, time-dependent stress tensor (electric and hydrodynamic). Cell electroneutrality and the spatial uniformity of $\langle\mathbf{E}\rangle$ require that the electric contribution to the outer surface integral vanishes. Evaluation of the hydrodynamic contribution (using definition 36) yields

$$Lh|_{r=b} = \frac{\gamma^2 b}{2}\left[\frac{\rho_p-\rho_s}{\rho_s}\phi\mu + \rho_s\left(\mu - \frac{2h(b)}{b}\right)\right] \qquad (57)$$

where ρ_p is the particle mass density. Substitution of eq 52 into eqs 57 and 55 yields

$$Lh|_{r=b} = \gamma^2\phi\left[\frac{\rho_p-\rho_s}{\rho_s}\right]h(b) \qquad (58)$$

and

$$\frac{\mathrm{d}}{\mathrm{d}r}[r(L+\gamma^2)h]|_{r=b} - 2\gamma^2h(b) - \frac{\rho_{el}^{(0)}(b)b}{\eta_s} = 0 \qquad (59)$$

respectively. Note that our set of equations differs from that of Carrique, et al.[32−36] only in the sense that we insist $P(b) = 0$, as a result of eq 53, while they insist that $Lh|_{r=b} = 0$, on the basis of the intuitive eq 46. However, it should be appreciated that our common use of eq 52 is based on different reasonings.

Equations 41, 44, 58, and 59 with their full physical motivations, together represent the principal novel contribution of this paper. The results described in the next section were found using these conditions together with 37, 38, and 39.

To orient the reader, we have summarized in Table 1 our self-consistent set of boundary conditions and compare these with some of the different boundary conditions that have been proposed in the past.

V. Computational Details

In our calculations, we find it convenient to introduce the following nondimensional variables: $x = \kappa r$, $x_a = \kappa a$, $x_b = \kappa b$, $Y = e\Psi^{(0)}/k_BT$, $\Phi_j = \kappa\phi_j$, $\Theta = \kappa\psi$, and $H(x) = \kappa h(r)/\mu_0$, where $\mu_0 = \epsilon_s\epsilon_0/\eta_s\ k_BT/e$. With the nondimensional parameters $m_j = \lambda_j\mu_0/e$, $\alpha_j = z_jn_j^\infty/\Sigma_jz_j^2n_j^\infty$ and $\beta_j = z_j\alpha_j$, and function definition $G = \Sigma_j\beta_j\exp(-z_jY(x))\Phi_j(x)$, the governing equations are then reduced to

$$\frac{1}{x^2}\frac{\mathrm{d}}{\mathrm{d}x}\left(x^2\frac{\mathrm{d}Y}{\mathrm{d}x}\right) = -\sum_{j=1}^{N}\beta_j\exp(-z_jY(x)) \qquad (60)$$

for the zeroth-order problem, and the simultaneous system

$$\begin{cases}\hat{L}\Theta - (\sum_j\beta_j\exp(-z_jY(x)))\Theta = G\\ \hat{L}H + \gamma^2H = Q,\\ \hat{L}Q = -\frac{1}{x}\frac{\mathrm{d}Y}{\mathrm{d}x}G,\\ \hat{L}\Phi_j + \gamma_j{}^2\Phi_j = z_j\frac{\mathrm{d}Y}{\mathrm{d}x}\frac{\mathrm{d}\Phi_j}{\mathrm{d}x} - 2m_j\frac{\mathrm{d}Y}{\mathrm{d}x}\frac{H}{x} - \gamma_j{}^2\Theta,\end{cases} \qquad (61)$$

where $\hat{L} = L/\kappa^2$ is the nondimensional version of L, and the second equation conveniently defines the new function Q. The

(43) Ascher, U.; Christiansen, J.; Russell, R. D. *COLSYS*; Netlib Repository of the Univeristy of Tennessee and Oak Ridge National Laboratory. http://www.netlib.org (accessed 2004).
(44) Preston, M.; White, L. R.; Kornbrekke, R. *Langmuir* **2005**, *21*, 9832.
(45) Carrique, F.; Cuquejo, J.; Arroyo, F. J.; Jimenez, M. L.; Delgado, A. V. *Adv. Colloid Interface Sci.* **2005**, *118*, 43.

boundary conditions at $r = a$ ($x = x_a$) are

$$Y(x_a) = e\zeta/k_BT \tag{62}$$

for the zeroth-order problem, and

$$\begin{cases} H(x_a) = 0, \\ \dfrac{dH}{dx}(x_a) = 0, \\ \dfrac{d\Phi_j}{dx}(x_a) = 0, \\ \dfrac{\Theta(x_a)}{x_a} - \dfrac{\epsilon_s}{\epsilon_p}\dfrac{d\Theta}{dx}(x_a) = 0 \end{cases} \tag{63}$$

for the first-order problem. At $r = b$ ($x = x_b$), the conditions are

$$\frac{dY}{dx}(x_b) = 0 \tag{64}$$

for the zeroth-order problem, and

$$\begin{cases} \Theta(x_b) = -x_b, \\ \Phi_j(x_b) = x_b, \\ Q(x_b) = \gamma^2\left(1 + \phi\dfrac{\Delta\rho}{\rho_s}\right)H(x_b), \\ \dfrac{dQ}{dx}(x_b) + Q(x_b)/x_b - 2\gamma^2 H(x_b)/x_b \\ -\sum_{j=1}^{N}\alpha_j \exp(-z_j Y(x_b)) = 0, \end{cases} \tag{65}$$

for the first-order problem.

The above coupled system of complex ordinary differential equations (odes), eq 61, subject to inner boundary conditions 63 and outer boundary conditions 65, are solved using a collocation method. As one means of ensuring correct results, two independent programs were used to perform the calculations. One was written in the Fortran 90 language and uses the COLSYS collocation package[43] to solve the above system of odes, in the same manner described in ref 44 to handle boundary value problems for stiff differential equations (which these equations become at sufficiently high frequencies[39,44]). A second program was written in the Matlab language, and utilizes the internal BVP4C routine, which is also a collocation algorithm. All cases shown (as well as others) were run with both packages with excellent agreement found when both sets of calculations converged. However, the Matlab program failed to converge with certain extreme combinations of high ζ potential, high electrolyte concentration, and low volume fraction. In contrast, the Fortran/COLSYS program converged in all cases studied. In terms of computational speed, the Fortran/COLSYS program converged a factor of 10−100 times faster than the Matlab version (when run on the same hardware). The Matlab version, however, has the advantage that it is more convenient given the availability and ease of accessibility of the MatlabledR software package. Our Matlab program is available upon request.

The solution of the first-order cell model clearly requires the solution of the zeroth-order cell model for supply of the Y function. Equation 60 with boundary conditions 62 and 64 is thus solved first, using the same technique, to give Y. After a final solution of the first-order system has been obtained, the complex electrophoretic mobility is determined a posteriori using

$$\frac{\mu}{\mu_0} = \frac{2H(x_b)}{x_b} \tag{66}$$

from eq 52.

VI. A Comparison between Cell Models

The dependence of the mobility modulus on the frequency of the applied field as predicted by the present model is represented by the thick solid curves in Figures 2−7. For convenience, all modulus results are shown in units of $\mu_0 = \epsilon_s\epsilon_0 k_B T/e\eta_s \approx 2 \times 10^{-8}$ m^2·s^{-1}·V^{-1}, that is, Smoluchowski's static mobility for a ζ potential of $k_BT/e \approx 25$ mV. Data for frequencies lower than those indicated tend to asymptote to values unique to the given system parameters and are of interest only in the sense that our model predictions agree in the limit of $\omega \rightarrow 0$ with published static data.[8] We have also confirmed (see dot−dashed lines in Figures 5−7) that, in the limit of very low volume fraction, $\phi \rightarrow 0$, our mobilities converge to those found for the case of an isolated spherical particle.[44]

With increasing ζ potential, our results clearly follow well-recognized trends. For low ζ potentials (Figures 2−4), the mobility modulus monotonically decreases with increasing frequency because the particles fail to keep up with the field oscillations as a result of their inertia.[28,36] This tendency persists, irrespective of both volume fraction, ϕ, and electrolyte concentration, κ. At medium to high ζ potentials (Figures 5−7), the mobility modulus first increases, exhibits a maximum, and then rapidly decreases with increasing frequency. This peak in mobility modulus, which becomes more pronounced as the ζ potential increases (compare, e.g., Figures 3 and 6 for a fixed $\kappa a = 10.4$ and fixed $\phi = 0.1$), is the manifestation of the Maxwell−Wagner−O'Konski (MWO) relaxation process.[36] Below the MWO relaxation frequency, the field-induced dipole coefficient of the particle (including its double layer) is controlled by the difference between the conductivities of the particle and the medium. Above that relaxation, it is controlled by the permittivity mismatch (it approaches −1/2 if $\epsilon_p \ll \epsilon_s$). At low ζ, the conductivity of the particle is low, and the dipole coefficient is approximately −1/2, which is below the MWO relaxation frequency. At high ζ, the coefficient may approach +1 at low frequency (if the surface conductivity is large enough) and −1/2 at high frequency. This decrease explains the observed increase in $|\mu|$.[36]

A comparison between the figures for a fixed ζ potential (i.e., between Figures 2−4 for $\zeta = 25$ mV or between Figures 5−7 for $\zeta = 100$ mV) shows that, in the range $\kappa a = 1$ to $\kappa a = 60$, the mobility increases monotonically with κa. This behavior was already described by Preston, et al.[44] for the case of an isolated spherical particle, but it is also seen here to be the case for any of the given finite volume fractions specified.[28,36]

In general, a finite concentration of colloidal particles introduces additional screening (above that of Debye screening) of the field felt by an individual particle. This leads to an overall reduction in the mobility modulus as the volume fraction, ϕ, increases. Carrique, et al.,[34] for example, summarize the situation by concluding that the stronger the particle−particle interactions, the lower the mobility. Generally speaking, at a fixed ζ, reducing κ (increasing the double-layer thickness) and increasing ϕ (diminishing the relative separation of particles) have the same effect of increasing the electrohydrodynamic interaction and thus reducing the mobility. While we can confirm Ohshima's conclusion[28] that, at a fixed frequency, the mobility tends to the static mobility as the volume fraction is increased by delaying the inertial decay, it is clear from Figure 4 that, at low ζ potentials, the mobility does not significantly increase with volume fraction

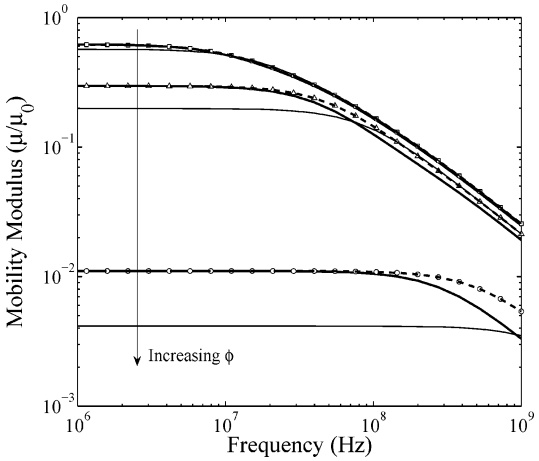

Figure 2. Dynamic mobility modulus versus frequency predictions as a function of field frequency of four cell models: this work (thick solid line), Carrique model (thick dashed line), Shilov−Zharkikh/Morse−Mehta model (thin solid line), and the Ohshima model (open symbols). The curves represent different volume fractions. From top to bottom: $\phi = 0.01$, 0.1, and 0.5. For clarity, we used different symbols for the Ohshima model (squares, triangles, and circles, respectively, for $\phi = 0.01$, 0.1, and 0.5). The parameter variables assumed are $\zeta = 25$ mV, a symmetric univalent electrolyte concentration $c_\infty = 10^{-5}$ M, and particle radius $a = 100$ nm. Thus, $\kappa a = 1.0$. Other system constants: $T = 298$ K, $\epsilon_s = 78.5$, $\epsilon_p = 10.0$, $\eta_s = 0.89 \times 10^{-3}$ kg/m·s, $\rho_s = 997$ kg/m^3, $\rho_p = 2400$ kg/m^3, $\Lambda_j^\infty = 75$ S·cm^2 for $j = 1$, 2, and $z_j = \pm 1$.

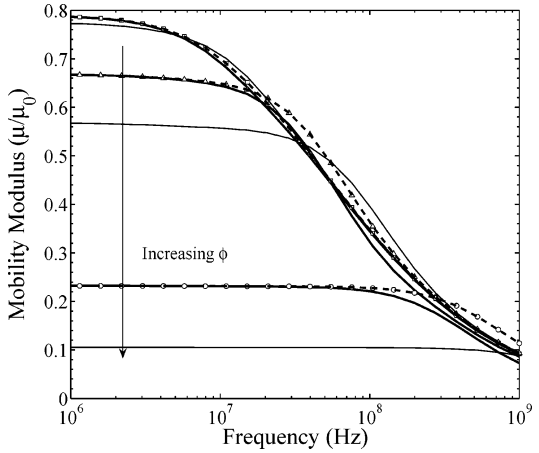

Figure 3. The same conditions shown in Figure 2, except $c_\infty = 1 \times 10^{-3}$ M and thus $\kappa a = 10.4$.

across a large range of frequencies (compare our results with Ohshima's predictions here and in Figure 7 of ref 28).

One criterion that must be fulfilled by any cell model is that its predictions must tend to the electrokinetic behavior of a single particle in the limit of zero volume fraction, $\phi \to 0$. Although, by construction, it is not possible to achieve this limit numerically while still complying with the assumptions of the cell model, it is nonetheless possible to approach the single particle results with decreasing volume fraction. Mobility modulus dependence on frequency for the isolated colloidal particle system, based on the calculation procedure of Preston, et al.,[44] are included in Figures 5−7 to represent this limit. These can be compared with our model predictions for concentrated particle systems of low volume fraction, $\phi = 0.01$, which can be considered good approximations to the isolated colloidal particle system. Clearly, the results of the present model with $\phi = 0.01$ are already in good agreement with the isolated particle limit. In fact, results (based on calculations using the Fortran/COLSYS program) for volume

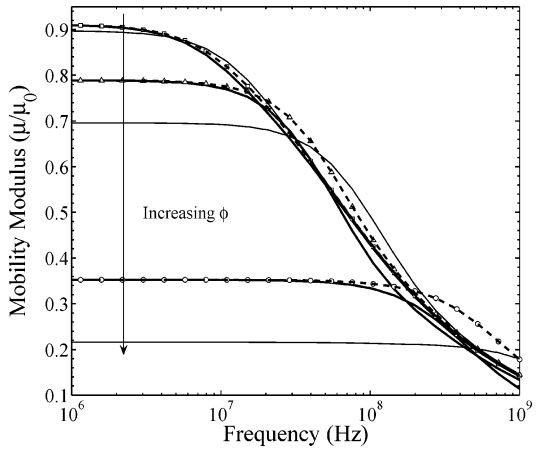

Figure 4. The same conditions shown in Figure 2, except $c_\infty = 3.125 \times 10^{-2}$ M and thus $\kappa a = 58.1$.

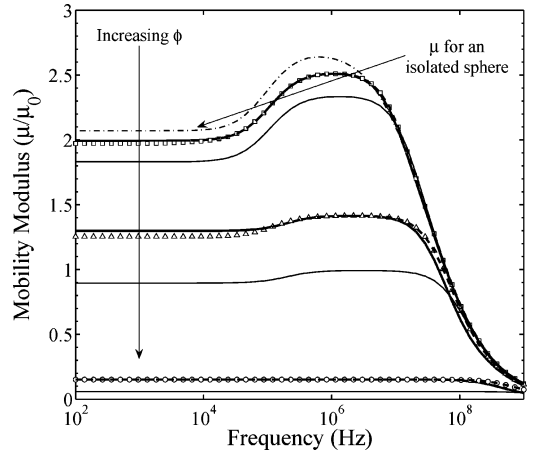

Figure 5. The same conditions shown in Figure 2, except $\zeta = 100$ mV, and the thin dot−dashed line represents the mobility modulus versus frequency prediction of Preston, et al.[44] for an isolated spherical particle under the same electrokinetic conditions.

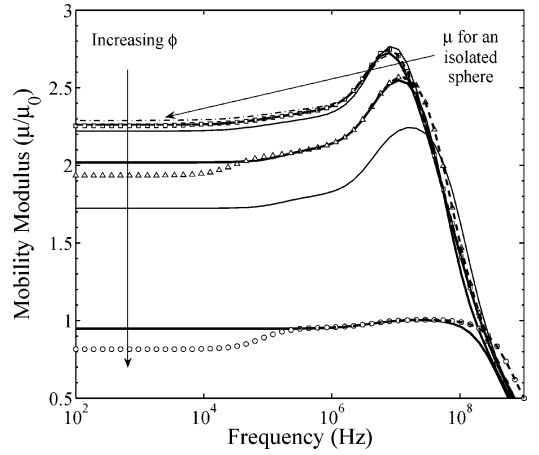

Figure 6. The same conditions shown in Figure 5, except $c_\infty = 1 \times 10^{-3}$ M and thus $\kappa a = 10.4$. Note that the range of mobility modulus has been restricted to increase clarity. The Shilov−Zharkikh/Morse−Mehta model prediction for $\phi = 0.5$ does not appear because it falls below the lower modulus limit.

fractions of $\phi = 0.001$ and $\phi = 0.0001$ are indistinguishable from the limiting values deduced by the Preston−White model. This in itself is a useful fact, considering that the single-particle calculations are considerably more involved[44] since they require the solution of the asymptotic problem as input to the numerical calculations. This suggests that the present finite volume fraction

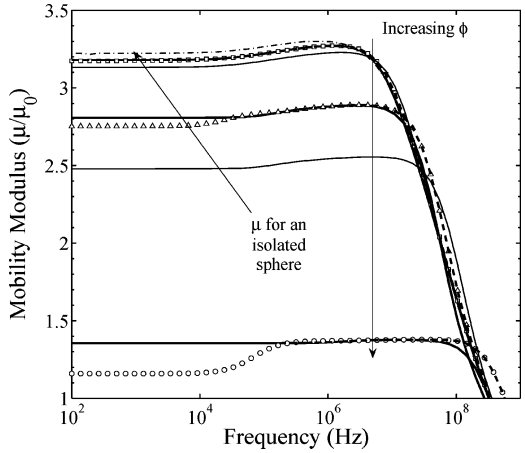

Figure 7. The same conditions shown in Figure 5, except $c_\infty = 3.125 \times 10^{-2}$ M and thus $\kappa a = 58.1$. Note that the range of mobility modulus has been restricted to increase clarity. The Shilov−Zharkikh/Morse−Mehta model prediction for $\phi = 0.5$ does not appear because it falls below the lower modulus limit.

algorithm, being simpler to implement, can be used even to obtain data for the isolated colloidal particle system.

Focusing now on the subject of boundary conditions, we compare the results obtained with the present cell model, which employs boundary conditions derived from global constraints, with results of cell models that adopt other boundary conditions. The latter are included in Figures 2−8. We restrict our comparison to the cell models most often referred to in the literature. Foremost of these are the Ohshima model[27,28] and the Carrique model.[32−36] We refer to these models in this manner for convenience only, but note the fact that the same models have also been advocated by other authors. For example, Shilov and Zharkikh[21,22] make reference to a cell model that employs conditions 46 and 52, as well as 41 and 44, and is thus the same as the above-named Carrique model. As an additional case for comparison, we consider the cell model based on the combination of the Shilov−Zharkikh[21,22] condition for the electrochemical potential 44 and the Morse−Mehta[42] condition for fluid velocity 48. This possibility, while not previously explored numerically in the literature, was nominated in the works of Shilov et al.[22,23] In the following, we refer to this model as the Shilov−Zharkikh/Morse−Mehta model. Since Ohshima defines dynamic mobility with respect to the external field rather than the average field as we do, we must multiply his mobility predictions by the factor $b/\psi(b)$ to make a consistent comparison with our mobility results (see Carrique, et al.[45] for a detailed discussion on this point).

The Carrique cell model largely agrees with the predictions of our model under the majority of situations studied. This is not surprising because there is considerable overlap in the set of boundary conditions employed by the two models. Numerically, these only show discernible differences at very high frequency, where the Carrique model predicts a slower decrease in mobility modulus with frequency due to a smaller inertial contribution. Not surprisingly, the Carrique model also tends to the isolated particle limit as $\phi \rightarrow 0$ (see Figures 5−7), as has already been confirmed in ref 36. The Carrique cell model has already been compared with both the Ohshima cell model[32] and with O'Brien's direct two-particle interaction model.[36] Both references document observed discrepancies. In the first instance, findings similar to those here (see below) were found. With respect to the comparison with the O'Brien theory, we remark that, after correction factors were introduced in both models,[36] the Carrique cell model was found to underestimate the inertial decay at very high frequencies relative to the O'Brien predictions. The correction factor of $1/(1 + \phi\Delta\rho/\rho_s)$ was applied to the cell model calculations to satisfy the condition of zero macroscopic momentum per unit volume.[13] This condition is inherently taken into account in eq 53.

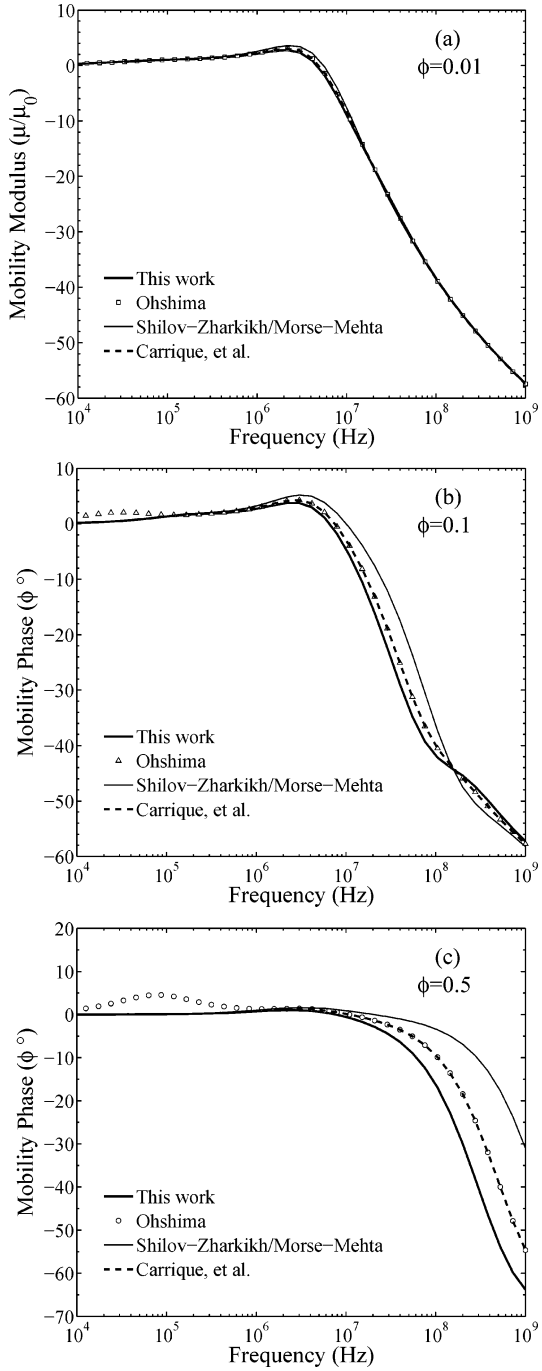

Figure 8. Plots of the mobility phase as a function of frequency. The physical conditions and line and symbol representations are the same as those in Figure 6. The ϕ values are as indicated in the respective figures.

It is of some interest to determine whether the overall agreement between our model and the Carrique model is fortuitous or due to our cell model numerically predicting the Kuwabara[41] hydrodynamic condition of zero vorticity at the outer cell boundary, used by the Carrique model. In Figure 9 we plot the magnitude of the complex function, $Lh(b)$, being the manifestation of boundary condition 46, against frequency for various conditions of κa and volume fraction, ϕ, at the high ζ potential of $\zeta = 100$ mV (note the log−log scale). For a considerable range of frequencies, κa values, and volume fractions, the condition that

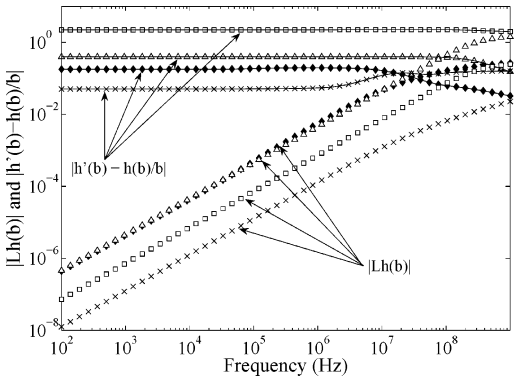

Figure 9. Plots of the modulus of the boundary values $Lh(b)$ (symbols) and $dh(b)/dr - h(b)/b$ (symbols with solid lines) as functions of frequency. These values are assumed to vanish in the Kuwabara and Morse−Mehta models, respectively. Deviations from zero are measures of the errors incurred. The symbols denote the following cases: $c_\infty = 1.0 \times 10^{-5}$ M ($\kappa a = 1.0$), $\phi = 0.01$ (solid diamonds) and $\phi = 0.5$ (open triangles); $c_\infty = 3.125 \times 10^{-2}$ M ($\kappa a = 58.1$), $\phi = 0.01$ (crosses) and $\phi = 0.5$ (open squares). All other system constants are the same as those in Figure 2, except $\zeta = 100$ mV.

$Lh(b) = 0$ is approximately upheld in practice. The data demonstrate a linear growth of $|Lh(b)|$ with frequency until, at very high frequencies, the function plateaus out at a finite value. The condition thus fails to hold at very high frequencies, which is where the disparity between the two cell models appears. One can infer from the fact that the condition is better satisfied under high κa conditions and best still at the lowest volume fraction that the condition is most appropriate when there is least electrohydrodynamic interaction between neighbor particles. Note that what has been plotted in Figure 9 is the magnitude of the complex $Lh(b)$. At low to medium frequency, this magnitude is dominated by the imaginary part of $Lh(b)$; the real part is several orders of magnitude smaller than the imaginary part.

Taking account of the difference in mobility definitions by means of the scaling factor $b/\psi(b)$ is essential for both qualitative and quantitative agreement between the Ohshima model and our predictions. Interpreting the Ohshima cell model mobility in terms of the average field instead of in terms of the external field leads to significantly erroneous results. Properly interpreted, the Ohshima model predictions essentially coincide at high frequencies with the Carrique predictions: note that both employ the Kuwabara boundary condition. At low frequencies, however, the Ohshima model has the potential to diverge from the Carrique model. Figures 2−4 suggest that, at low potentials, the two models remain consistent across a large frequency range ($[10^2, 10^9]$ Hz). However, Figures 5−7, representative of higher potentials, show that the Ohshima model suddenly deviates from the Carrique model, and therefore also from our model, at low frequencies as the volume fraction is increased. Indeed, under the conditions of these figures, the Ohshima model has quantitatively incorrect steady-state asymptotes. In summary, the boundary conditions employed in the Ohshima model are valid at low frequencies under low surface potential conditions, but fail under high potential conditions, specifically because of the electrostatic boundary condition used. On the other hand, the high-frequency deviations from our model predictions are instead due to failure of the Kuwabara condition. There are analogous deviations in the mobility phase, as demonstrated by Figure 8.

In contrast, the Shilov−Zharkikh/Morse−Mehta cell model shows little tendency to agree with our (or the Carrique or Ohshima cell model) predictions, except under very low volume fraction conditions. In the majority of the cases shown in Figures 2−7, only for $\phi = 0.01$ does the model more or less exhibit the same qualitative and quantitative behavior as ours. A particular point to note is that the correct static limits are not realized by this model. The overall impression obtained from a comparison across the spectrum of system parameters represented in Figures 2−7 is that the Morse-Mehta condition consistently underestimates the mobility response with frequency, but always demonstrates the correct qualitative features. In fact, there seems to be a simple monotonic, ϕ-dependent factor between this model and ours. However, we have not thought it worthwhile to investigate the nature of this factor.

In Figure 9, we have also quantified our model predictions of the Morse−Mehta boundary condition, eq 48, which is equivalent to the function $dh(b)/dr - h(b)/b$ vanishing. The magnitude of this function is plotted against frequency for the same system conditions as for the above Kuwabara study. Clearly, our cell model fails to substantiate the assumed boundary condition. The best case scenario is again under low volume fraction and high κa conditions, pertaining to systems with low particle interactions. In contrast to the Kuwabara case, this function seems largely independent of frequency. A similar investigation of Ohshima's electric potential condition $d\psi/dr = -1$ at $r = b$ produces quantitatively very similar results and frequency dependence (data not shown for clarity). That is, this condition is also not substantiated by our model in any of the cases tested. As we have seen, however, interpreting the mobility in terms of the external field rather than the average field and adjusting the model accordingly by means of the factor $b/\psi(b)$, brings Ohshima's calculation in line with the Carrique model at moderate to high frequencies under all of the conditions studied here. Since we have established that our model predictions agree well with those of the Carrique model and that the Kuwabara condition is valid in the range of low to moderately high frequencies, the discrepancy between the Ohshima model and both our model and the Carrique model at low frequencies points to Ohshima's assumption that $d\psi/dr = -1$ at $r = b$ as being the major limitation of his model in that regime.

VII. Summary and Conclusion

In this paper we argue that use of the cell model in an electrodynamic context requires implementation of a self-consistent set of boundary conditions. Previous models of the dynamic electrophoresis of concentrated colloidal particle systems have employed boundary conditions based on intuitive arguments and are not guaranteed to be correct. We have derived a complete set of conditions based on a global averaging principle consistent with the use of the cell model itself. It transpires that some previously used boundary conditions, while incorrectly or insufficiently motivated, are, in fact, reproduced in this rigorous analysis, while others are not featured at all in our reasoning. In the former case, our global averaging principle gives these conditions new-found credibility. Naturally, the numerical predictions of the current model are generally consistent with those of models that employ similar conditions, specifically the Carrique model, but can differ significantly from those of other cell models.

We have also shown that the principle of determining the true outer cell boundary conditions from global average constraints does not exclude the possibility that other conditions, motivated by physical or symmetry arguments, can turn out to be quantitatively confirmed. This was demonstrated by the specific example of the Kuwabara condition, eq 46, being valid in practice at low to moderate field frequencies.

In a follow-up paper, we compare the new self-consistent cell model with electrokinetic experiments on a concentrated disper-

sion of identical particles. Further efforts using the self-consistent cell model will also include a study of the high-frequency conductivity of porous plugs. In that work, we shall also compare the present cell model with exact results based on periodic arrays of spherical particles. Such a comparison would shed further light on the validity of the boundary conditions presented herein.

LA0607252